TRANSVERSE LOADING AND RESPONSE OF LONG ROD PENETRATORS DURING HIGH VELOCITY PLATE PERFORATION

JEROME D. YATTEAU, GUNNAR W. RECHT, and KARL T. EDQUIST

Applied Research Associates, Inc., 5491 S. Middlefield Road, Suite 100, Littleton, Colorado 80123, USA

Summary—This paper describes the development of mechanically coupled engineering models to predict transverse loading and response of long rod penetrators associated with high velocity perforation of thin to moderately thick plates. Test results for L/D = 20 tungsten alloy rods are presented to illustrate the distinct effects of impact yaw and obliquity on terminal ballistic transverse loading and response of rod penetrators. The yaw effects loading model considers the plate cutting contact force that travels down the side of the rod when yaw is sufficient for contact with the edge of the breaching hole. The obliquity effects model addresses transverse loading due to asymmetric pressure relief as the rod approaches the rear surface and exits the plate. In both cases, the loading is presumed to be impulsive and three-dimensional vector relationships are used to account for the complex encounter geometries associated with arbitrary combinations of impact yaw and obliquity. The response model includes predictions of rod deformation and fracture and post-perforation linear and angular velocity vectors of the residual rod. Model predictions are compared with test results for titanium and tungsten alloy rods. © 1999 Elsevier Science Ltd. All rights reserved.

INTRODUCTION

Long rod penetrators are being considered for use in anti-air missile warheads. The targets and encounter conditions of interest require that the rods perforate multiple spaced target elements with impact obliquities up to 85° and at speeds up to 4 km/sec. The rods will normally be yawed to some extent upon impact depending on deployment orientation and the direction of the relative impact velocity vector. Combinations of impact yaw and obliquity result in penetration force components normal to the rod axis which can produce trajectory deflections, post-impact rod tumbling, and rod deformation and fracture. Axial loading penetration models are well developed and provide accurate mass and velocity loss predictions for unyawed rods and normal impact obliquities. However, penetration predictions for spaced target elements that do not also account for transverse loading effects will generally produce overly optimistic predictions of rod lethality. This paper describes the development of new engineering models to quantify transverse loading and response of rod penetrators for application to spaced plate penetration problems involving any combination of impact obliquity and impact yaw. The new models have been installed in the FATEPEN penetration computer code as part of an effort to extend its applications to long rod penetrators (Yatteau, et al. [1]). The current work extends an earlier modeling effort to predict post-impact tumbling behavior for long titanium rods perforating aluminum plates (Zernow [2], and Yatteau [3]).

TERMINAL BALLISTIC TRANSVERSE LOADING AND RESPONSE
CHARACTERISTICS FOR LONG ROD PENETRATORS

Impact Yaw Effects

Figure 1 contains multiple exposure radiographs illustrating the effects of increasing impact yaw on terminal ballistic response for tungsten alloy rods perforating steel plates at normal impact obliquity. The yaw angle entries below each set of images in Fig. 1 provide the measured yaw angle projections in the elevation and plan view orthogonal x-rays for each test (only one view is shown for each test). A positive elevation yaw angle corresponds to the nose down orientation and a positive plan view yaw angle corresponds to the nose up. Photographs of the target plate perforations for each test, as viewed normal to the impact face, are included in Fig. 1 to the right of the radiographs. The diameter, D_T, of the round breaching hole in the plates is indicated below the plate images. The darker rod images overlaying the radiographs in Fig. 1 correspond to FATEPEN model predictions for the measured impact conditions and are discussed below after presentation of the transverse loading and response models.

The rods in Fig. 1 punched circular holes in the plates 2.4 times larger than the rod diameter and lost 11% of their length at the nose to axial erosion and extrusion-shear mass loss mechanisms. The rod in the top set of images impacted with a total yaw of only 1.8° which was just sufficient for the tail of the rod to graze the edge of the 10.5 mm hole during passage through the plate (the computed initial contact force location and direction on the rods are indicated by the normal contact force vector, Fc, on the predicted rod images). The tail contact is evident by the slight indent in the edge of the hole in the plate at the 10 o'clock position. There is no noticeable trajectory deflection and only a small post-impact tumble rate is apparent in the post-impact radiographs. The rod in the middle set of radiographs in Fig. 1 impacted with a larger total yaw angle of 3.9° which, together with the measured hole size, indicates that the side of the rod first contacted the edge of the hole at about mid-length. The portion of the rod aft of this point then cut a slot in the steel plate as it passed through the plate. The slot length indicates that rod orientation did not change significantly during passage through the plate. The post-impact trajectory deflection, tumble direction, and rod deformation are all consistent with the slot cutting force tracking along the rear half of the rod, normal to the rod axis, in the yaw plane and directed along the length of the slot toward the axis of the rod. The test in the lower radiographs in Fig. 1 involved an impact yaw of 6° which causes an earlier first contact with the edge of the hole as indicated. The slot length in the target is correspondingly longer and the trajectory deflection, post-impact tumble rate, and rod deformation are all more severe as a result of the larger cutting force component normal to the rod axis.

In general, for normal impact obliquity, the impacting end of a rod penetrator will produce an enlarged circular hole in the plate. The degree of hole enlargement over the diameter of the rod is a critical factor affecting transverse loading and depends on the plate material and increases with increasing plate thickness and impact speed (Yatteau [4]). Depending on the amount of hole enlargement, the rod L/D, and the impact yaw, the side of the rod may contact the edge of the hole at a point behind the nose during passage through the plate. When this "delayed contact" occurs, the rod will cut a slot in the plate and the cutting force will track down the remaining length of the rod giving rise to a trajectory deflection, post-impact tumbling, and possibly deformation and fracture of the rod.

Impact Obliquity Effects

The photographs in Fig. 2 illustrate rod response and plate damage for nearly unyawed tungsten alloy rods perforating steel plates at increasing impact obliquity. At the 45° impact obliquity, the rod lost approximately 20% of its length to axial loading erosion and extrusion-

shear mechanisms and the transverse loading produced a noticeable bend in the rod. There is very little post-impact tumbling of the rod in the elevation view radiograph. At the 75° impact obliquity, the rod lost approximately 40% of its length and was bent more severely by the transverse loads. In both sets of radiographs, rod deformation appears to continue between the two images behind the targets. Part (but not all) of the apparent deformation for the 75° impact obliquity is due to a slight post-impact rotation (roll) of the curved rod about the shotline. Also in this case, the rod appears to have pitched in the counter-clockwise direction contrary to expectations. The unexpected rotation direction is most likely a reaction to contact between the rear of the rod and the edge of the hole due to rotation in the plate.
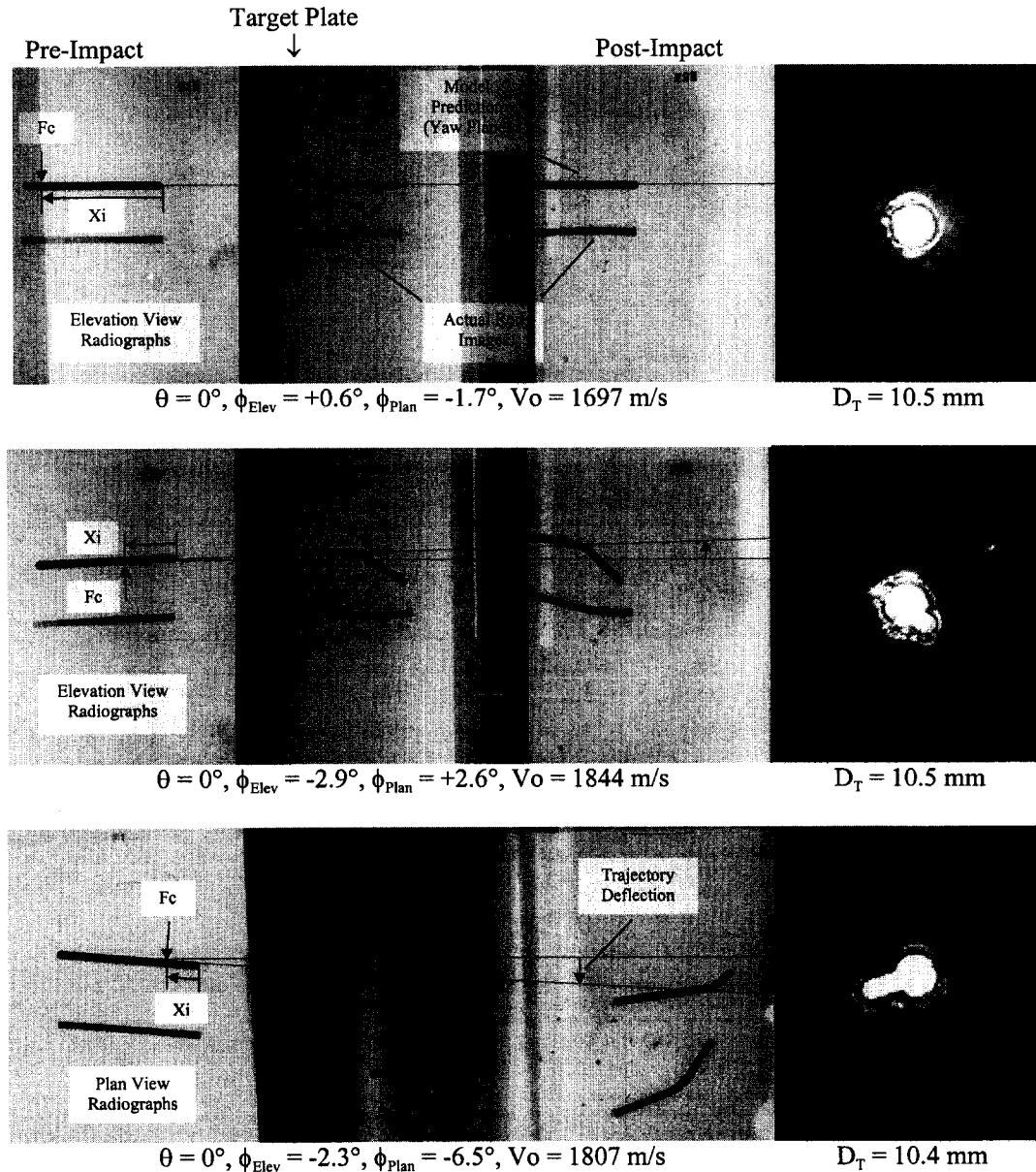

Fig. 1.   Effects of increasing impact yaw on rod deformation, trajectory deflection, and post-impact tumble rate. Tungsten alloy rods (R_c30, $D = 4.75$ mm, $L/D = 20$) vs. 1018 CR steel plates (BHN 90 - 110, $T/D = 2$) normal impacts.
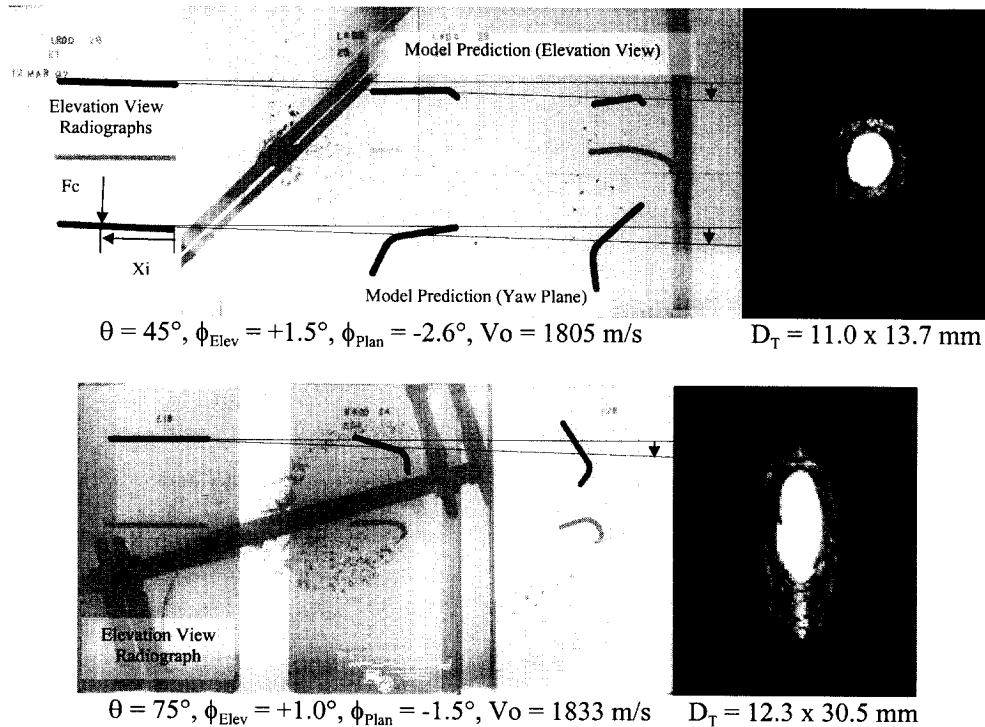
Fig. 2.   Effects of increasing impact obliquity on rod deformation, trajectory deflection, and post-impact tumble rate. Tungsten alloy rods (R_c30, $D = 4.75$ mm, $L/D = 20$) vs. 1018 CR steel plates (BHN 90 - 110, $T/D = 2$).

Figure 3 contains rod and plate penetration pressure contours for an $L/D = 10$ tungsten alloy rod perforating a $T/D = 2$ steel plate at 45° impact obliquity. The CTH code predictions confirm that pressure relief from the rear surface of oblique plates produces an asymmetric pressure distribution and transverse force component on the nose of the residual penetrator as it emerges from the rear surface. The impulse of the resultant transverse force component is the source of post-impact trajectory deflections, tumbling, and deformations observed in unyawed penetrators during oblique plate perforation. Finally, the obliquity plane cross section of the hole in Fig. 3 reveals an offset between the centerline of the rod and the center of the hole when projected onto the plane normal to the velocity vector (projection plane). The direction of the offset is given by the projection of entry side, outward, plate normal on the projection plane. The hole offset for oblique impacts introduces a dependence of the delayed contact location for yawed rod impacts on the location of the yaw plane relative to the obliquity plane.

Comparisons of the trajectory deflections for normal and oblique impacts reveals that the transverse impulse on the rod due to the yaw effect slot cutting, when it occurs, generally dominates the obliquity effect with regard to trajectory deflection and post-impact tumbling. However, as will be seen in what follows, the obliquity effect becomes significant at speeds near the ballistic limit velocity.
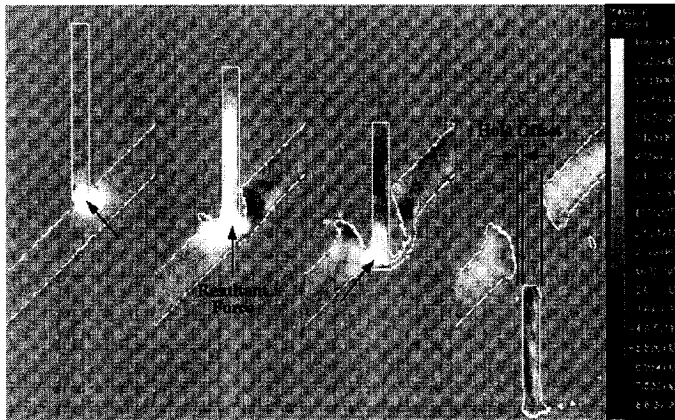
Fig. 3. Three-dimensional CTH simulation results illustrating effects of
impact obliquity on penetration pressure distribution and offset
between hole center and rod axis. Tungsten alloy rod (R_c30, L/D = 10)
vs. mild steel plate (θ=45°, T/D = 2), V = 1524 m/s.

TRANSVERSE LOADING MODEL

The transverse loading and response models are based on the linear and angular impulse -
momentum principles with empirical elements introduced to account for unknown material
response characteristics. An underlying assumption in the model development is that the loading
is impulsive. That is, the passage of the rod through the plate is recognized in the loading
geometry but the orientation of the rod is presumed not to change during the penetration.

Impact Yaw Effects

The sketch in Fig. 4 illustrates the delayed contact loading model for a yawed rod penetrator
perforating a thin plate. The nose of the rod breaches the plate creating a hole with diameter, D_t,
which is larger than the diameter, D_c, of the rod. In the process, the rod length has been reduced
from L to L_r and the velocity and angular momentum vectors have been changed from $\bar{V}$ to $\bar{V}_r$
and $\bar{L}$ to $\bar{L}_r$. The pre-impact yaw angle, ϕ, causes the side of the rod to initially contact the
edge of the hole a distance X_i from the nose of the residual rod. As the rod continues through the
plate, the rear of rod cuts a slot in the plate, and the cutting force, $\bar{F}_c$, tracks down the side of the
rod.

The principal elements of the yaw effects loading model include the diameter, D_t, of the
breaching hole, the magnitude and direction of the cutting force, $\bar{F}_c$, the initial delayed contact
location, X_i, the cutting force tracking speed, $\dot{X}$, down the side of the rod, and the cutting speed,
C_s, in the plate. The hole diameter, D_t, is provided by the existing FATEPEN hole size model as
a function of target material and thickness and the impact velocity (Yatteau [4]). The cutting
force vector is computed to be the product of a modified hydrodynamic flow pressure and the
bearing area, A_c, between the rod and target plate.

$$\bar{F}c = \left[\sigma_{ct} + \tfrac{1}{2}\rho_t C_d (V \sin \phi)^2\right] A_c \bar{e}_f \tag{1}$$

where σ_{ct} is the effective target material flow stress for slot cutting, ρ_t is the target density, C_d, is
the drag coefficient for flow about the side of a cylinder (C_d = 0.5), and V is the rod velocity.
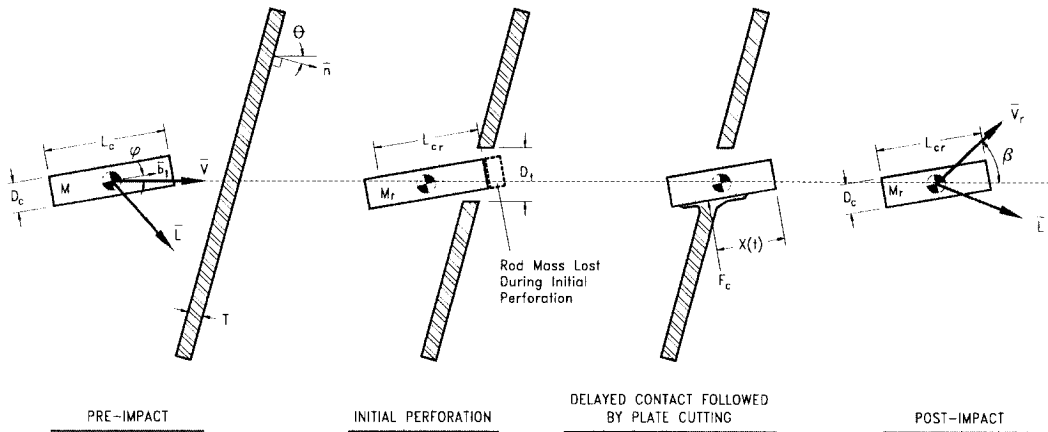
Fig. 4. Transverse loading due to impact yaw (delayed contact).

Friction forces between the rod and plate are neglected in computing the dynamic pressure in Eqn. (1) and thus only the normal component of the relative flow velocity is used.

The cutting force bearing area, A_c, is given by

$$A_c = T_c D \tag{2}$$

where T_c is the width of the plate in contact with the rod

$$T_c = \frac{T}{\overline{b}_1 \bullet \overline{n}} \tag{3}$$

where ($\bullet$) denotes the scalar product, and T is the normal plate thickness.

The effective flow stress, σ_{ct}, is assigned a value between the dynamic yield strength for uniaxial stress, σ_{yt}, and the modified hydrodynamic penetration theory flow stress for confined penetration of semi-infinite plates, R_t. The assignment is determined by interpolation between σ_{yt} and R_t based on T_c / D. The cutting force acts in the yaw plane normal to the rod axis. The unit vector defining the direction of the cutting force on the rod is given by the vector products

$$\overline{e}_f = (\overline{e}_v \times \overline{b}_1) \times \overline{b}_1 \tag{4}$$

where ($\times$) denotes the vector product, $\overline{e}_v$ is a unit vector along the velocity vector and $\overline{b}_1$ is the unit vector along the rod axis.

Details of the rod/plate encounter geometry are illustrated in Fig. 5 for a yawed rod penetrating an oblique plate with arbitrary orientations for the yaw and obliquity planes. The location of the initial contact point on the side of the rod, X_i, for any impact yaw and obliquity, can be reduced to

$$S_c = \left[\sqrt{\left(\frac{D_t}{2}\right)^2 - (S_h \operatorname{Sin}\alpha)^2} + S_h \operatorname{Cos}\alpha - \left(\frac{D}{2}\right) \operatorname{Cos}\alpha\alpha \right] \tag{5}$$

$$X_i = \frac{S_c}{\operatorname{Sin}\phi} \tag{6}$$

where α is the angle between the intersections of the yaw and obliquity planes with the projection plane (Fig. 5) and S_h is the hole offset due to the impact obliquity (Fig. 3) given by

$$S_h = \frac{(D_t - D)}{2} \mathrm{Sin}\theta \qquad (7)$$

which provides the maximum offset at the theoretical obliquity of 90° and no offset at normal impact obliquity. The cutting force tracking speed down the rod is

$$\dot{X} = V \frac{\mathrm{Sin}(\phi + \delta)}{\mathrm{Sin}\delta} \qquad (8)$$

and the speed of cutting in the plate is

$$C_s = V \frac{\mathrm{Sin}\phi}{\mathrm{Sin}\delta} \qquad (9)$$

where δ is the acute angle in the yaw plane between the rod axis and the plane of the plate.

As the rod approaches parallelism with the plate (δ approaches zero), the cutting speed increases without bound. When the cutting speed in the plate exceeds the hole growth rate there can be no delay in contact with the plate. In the absence of a hole expansion rate formula, it is assumed that a lower bound for the hole growth rate is provided by the target material plastic wave speed for uniaxial stress, U_{PT}, and an upper bound is provided by the target Hugoniot wave speed, U_{HT}. A cosine function interpolation formula, with C_s/U_{HT} as the independent variable, is used to reduce the initial delayed contact location, X_i, to zero as C_s increases between U_{PT} and U_{HT}. Thus, when $C_s \geq U_{HT}$, X_i is zero which corresponds to continuous contact between the rod and plate. If $Cs \leq U_{PT}$ the delayed contact location is given by the maximum value from Eqn. (6).
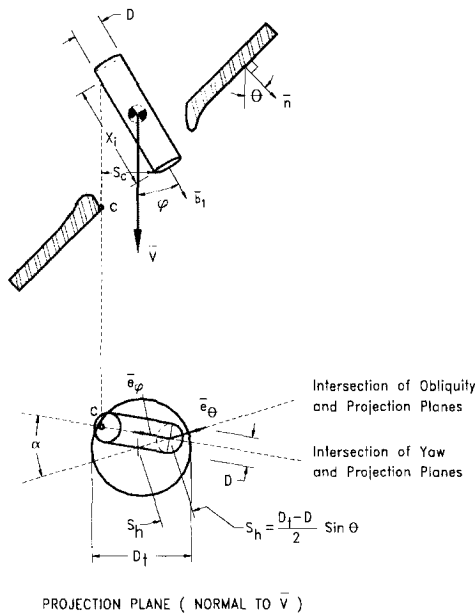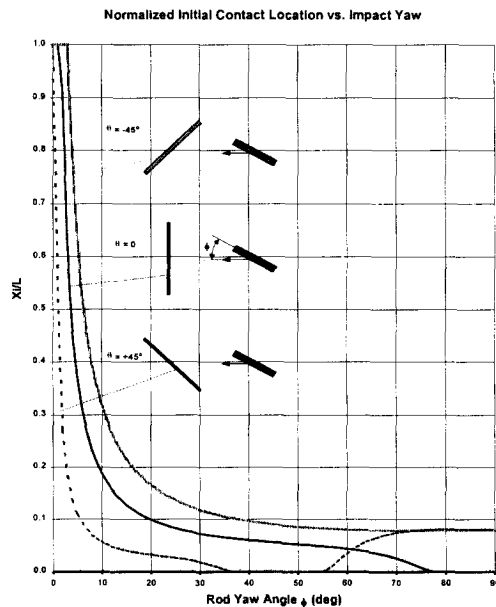

Fig. 5. Delayed contact rod/plate encounter geometry.

Fig. 6. Normalized initial contact distance vs. impact yaw , L/D = 16 titanium rods vs. aluminum plates, T/D = 1.16, V = 1525 m/s, D_T/D = 1.84.

Typical variations in X_i (normalized by the rod length, L) with impact yaw and obliquity are plotted in Fig. 6. In this example, the yaw and obliquity planes are coincident. In all three cases the rod nose is pitched up relative to the velocity vector. The three curves reveal how quickly the initial contact point shifts towards the nose (and continuous contact) with increasing yaw and also illustrate the effects of the impact obliquity hole offset and cutting speed on the variation in X_i. For the normal obliquity, the rod approaches parallelism with the plate as the yaw angle nears 90° and X_i falls to zero (continuous contact) at a yaw angle near 75° due to the cutting speed effect. For the negative obliquity angle (top of plate tilted up-range), the rod contacts the near edge of the offset hole at nearly zero yaw. Also in this case the rod approaches parallelism with the plate surface when the yaw angle approaches 45° and the cutting speed effect reduces X_i to zero for yaw angles between 35° and 55°. Finally, for the +45° obliquity, the side of rod contacts the far edge of the offset hole at a larger yaw angle near 3° and the rod does not approach parallelism with the plate in the 90° yaw range in Fig. 6.

Impact Obliquity Effects

Transverse penetration force components associated with impact obliquity arise from the shift in the penetration pressure resultant from alignment along the rod axis toward alignment with the rear face of the plate as illustrated in Fig. 3. In the current development, we have not attempted to explicitly model the obliquity effect transverse loading from the complex and time-dependent local flow fields in the penetrator and target as the rod approaches the rear surface. Instead, we have adapted a previously developed correlation for obliquity effects trajectory deflection in terms of the impact velocity normalized by the ballistic limit velocity as shown in Fig. 7 (Recht [5]). Figure 7 contains trajectory deflection angle data for compact steel cylinders (L/D = 1) perforating relatively thin (T/D = 0.25-0.29) mild steel and aluminum plates. Because of their short length and most likely small or zero impact yaw angles (the cylinders were probably spin-stabilized fragment simulating projectiles) the trajectory deflection data in Fig. 7 are presumed to be uncomplicated by any delayed contact yaw effects loading. The correlation for the obliquity effect trajectory deflection angle, β_θ, in terms of V/V_{50} derives from application of the impulse-momentum principle to the ideal plate-plugging geometry sketched in Fig. 7 together with the assumption that the penetration forces on the cylinder due to plate strength effects are rate independent. The formula for β_θ in Fig. 7 has been found to provide reasonably good predictions for unyawed rod penetrator trajectory deflections and is utilized in FATEPEN to estimate the obliquity effect transverse loading contribution to the overall rod linear and angular momentum changes and rod deformation as described below. Note that when the penetrator impacts at just above the ballistic limit velocity (X=1), $\beta_\theta = \theta$ corresponding the largest obliquity effect transverse loading impulse.

RESPONSE MODEL

Trajectory Deflection

In determining the overall trajectory deflection angle, β, it is assumed the obliquity effects loading on the nose of the rod occurs prior to the delayed contact loading due to yaw. The vector change in rod velocity due to the obliquity effect is given by

$$\overline{\Delta V}_\theta = V_{r(\phi=0)}\overline{e}_{vr'} - V\overline{e}_v \tag{10}$$
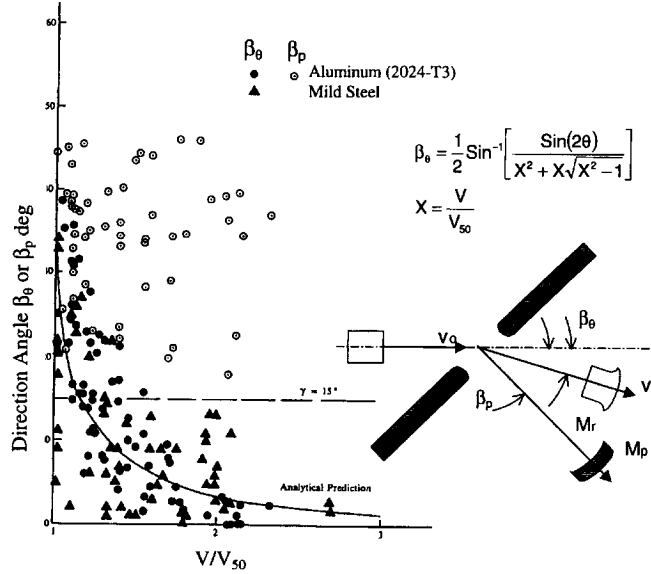
Fig. 7.   Obliquity effect penetrator and plate plug trajectory deflections for compact steel
cylinders perforating steel and aluminum plates. Impact obliquity = 45° (Ref. [5]).

where $V_{r(\phi=0)}$ is the magnitude of the residual velocity for the unyawed rod as computed using the axial loading models resident in FATEPEN, V is the impact velocity, $\bar{e}_{vr'}$, is a unit vector along the deflected trajectory after the obliquity effect loading , and $\bar{e}_v$ is the unit vector along the impact velocity vector. The $\bar{e}_{vr'}$, unit vector is presumed to lie in the obliquity plane ($\bar{e}_v$- $\bar{n}$ plane) rotated by the angle, β_θ (Fig. 7), from $\bar{e}_v$ toward the plate normal.

The trajectory deflection, β_ϕ, due to yaw effects defines the deflection of the residual velocity vector from $\bar{e}_{vr'}$ to its final orientation along $\bar{e}_{vr}$. The change in velocity due to the slot cutting force, $\bar{F}_c$, tracking down the side of the rod is determined by

$$X_{ir} = X_i - (L - L_r)$$ (11)

$$\overline{\Delta V}_\phi = \left(\frac{L_r - X_\pi}{\dot{X}_r}\right)\frac{\overline{F}c}{Mr}$$ (12)

where X_{ir} is the position of the initial contact on the side of the residual rod of length L_r, as determined by the axial loading residual mass model, $\dot{X}r = \dot{X}\cdot(V_{r(\phi=0)}/V)$ is the adjusted force tracking speed, and M_r is the rod residual mass. The force, $\bar{F}_c$ (Eqs. 1-4) is also computed after accounting for the obliquity effect on the rod velocity. The change in velocity, ΔV_ϕ, is limited to the component of the initial impact velocity normal to the rod axis to reflect that the cutting force drops to zero when the rod lifts off the bottom of the slot. The residual velocity vector after combined obliquity and yaw effects loading and the overall trajectory deflection, β (and β_ϕ), are obtained by simple vector addition of $\bar{V}$, $\overline{\Delta V}_\theta$ and $\overline{\Delta V}_\phi$.

Post-Impact Tumbling

FATEPEN computes changes in penetrator orientation between impacts from the penetrator residual angular momentum vector , $\bar{L}_r$. The change in angular momentum due to the yaw effect is given by the angular impulse of the cutting force on the residual rod (see Fig. 4)

$$\overline{\Delta L}_\phi = \int_{x_i}^{L_r} \left[\frac{L_r}{2} - x(t) \right] \overline{b}_1 x \overline{F}_c \frac{dx}{\dot{x}} \tag{13}$$

which, after integration reduces to

$$\overline{\Delta L}_\phi = \left(\frac{-x_{ir}}{2} \right) \overline{b}_1 x M_r \overline{\Delta V}_\phi \tag{14}$$

The change in rod angular momentum due to the impact obliquity effect is computed by assuming the effective moment arm of the transverse force component in this case is confined to the deformed nose and specifically the mid-point of the leading caliber of the residual rod length. The corresponding moment of the change in linear momentum can be written

$$\overline{\Delta L}_\theta = \left(\frac{L_r - D}{2} \right) \overline{b}_1 x M_r \left[\overline{\Delta V}_\theta - (\overline{\Delta V}_\theta \bullet \overline{e}_v) \overline{e}_v \right] \tag{15}$$

where the term in brackets reflects the assumption that the component of ΔV_θ (for an unyawed rod, Eqn. (10)) in the direction of the impact velocity vector does not contribute a net angular impulse to the rod (i.e, the associated forces act along the axis of the rod and any associated mass loss is expelled symmetrically about the axis of the rod). The residual angular momentum and angular velocity after the combined yaw and obliquity are obtained from the vector addition of $\overline{L}$, $\overline{\Delta L}_\phi$, and $\overline{\Delta L}_\theta$.

Rod Deformation and Fracture

Rod deformations and fracture are estimated using a modified version of the plastic shear wave propagation model developed by Recht [6] to estimate deflection profiles in plates impacted by cylinders at speeds below the ballistic limit velocity. Adaptation of Recht's model to rod deformation due the impact obliquity effect is illustrated by deforming rod sketches in Fig. 8. The nose mass, M_n, is presumed to be impulsively loaded by the obliquity effect force and achieves an initial velocity, V_n, normal to the axis of the rod given by

$$V_n = \frac{M_r}{M_n} \Delta V_\theta \tag{16}$$

The relative motion of the nose is accommodated by rod deformations associated with the propagation of a plastic transverse or shear deformation wave moving at speed U_τ relative to the undeformed rod. Displacements due to elastic waves (tensile and shear) moving ahead of the plastic wave are neglected. The plastic wave speed, U_τ, is presumed to be constant which is consistent with an assumed bilinear, elastic-plastic, true stress- true strain curve for the rod material. The rod material ahead of the plastic wave is acted upon by a shear stress equal to the dynamic shear strength (bending moment effects are currently neglected in the model). Conservation of momentum dictates that the velocity of the deformed material behind the plastic shear wave decreases. As a result, the shear strain just behind the wave also decreases continuously and the rod material deforms only once on passage of the shear wave. Thus at any given time, all the deformed material and the nose mass have the same velocity V. The impulse-momentum principle applied to the deforming rod provides

$$M_n V_n = (M + M_n) \ V + \int_0^t \frac{\pi D^2}{4} \tau_y dt \tag{17}$$

X/D

Representative Fracture Shear Strains[7]
(10^2 S^{-1} Shear Strain Rate)

Material	Fracture Shear Strain (gam)
OFHC Copper (Rf 32)	>7
Armco IF Iron (Rf 71)	4.5
1006 Steel (Rf 94)	3.5
RHA (Rc 30)	0.9
2024 Aluminum (Rc 75)	0.45
S-7 Tool Steel (Rc 50)	0.4
Du-.75Ti (Rc 45)	0.2

Initial Velocity Distribution

Shear Wave Propagation

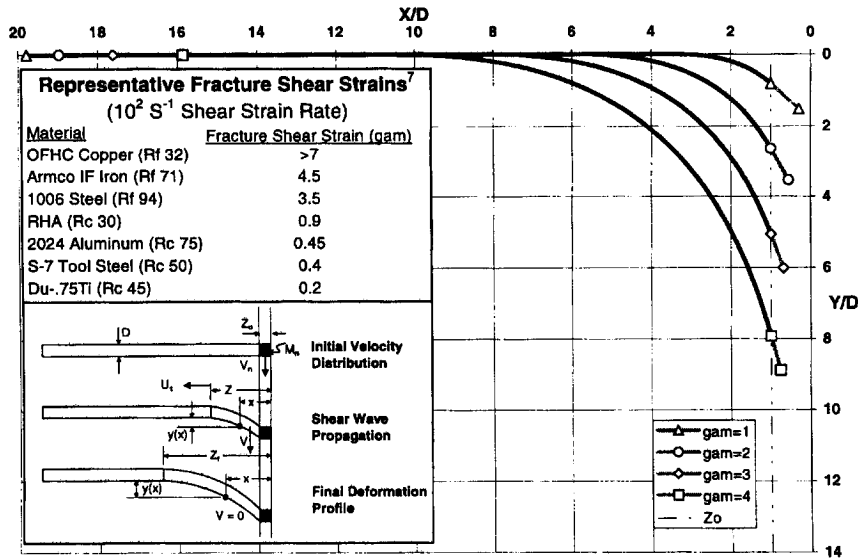Final Deformation Profile

Y/D

gam=1
gam=2
gam=3
gam=4
Zo

Fig. 8.   Shear deformation profiles for L/D = 20 rods corresponding to assumed initial shear strains of 1 - 4.

where we have neglected accelerations in the undeformed portion of the rod due to elastic shear wave reflections between the tail of the rod and the plastic shear wave front, and where M is the mass of the deformed rod between the wave front and the nose mass given by

$$Z = U_\tau t, \quad M = \frac{\pi D^3}{4} \rho \left(\frac{Z}{D} - \frac{Z_o}{D} \right) \quad (18)$$

A change of variables from t to Z in Eqn. (17) followed by double integration leads to the deformation profile of the rod as a function of the wave position, Z. Plastic deformation ceases when the velocity, V, of the deforming material falls to zero. The final deformed profile of the rod is given by

$$j = \frac{M_n}{\frac{1}{4}\rho\pi D^3} , \gamma_\theta = \frac{V_n}{U_\tau} , k = \frac{\tau_y}{\rho U_\tau^2} , i = \frac{\gamma_\theta}{k} , x' = \frac{x - Z_o}{D} , \frac{Z_f}{D} = \frac{Z_o}{D} + ij \quad (19)$$

$$\frac{y(x')}{D} = k \left\{ j(1+i) \ln \left[\frac{j(1+i)}{j+x'} \right] - ij + x' \right\} \quad (20)$$

where j is the ratio of the nose mass to the mass of one caliber of rod length, γ_θ is the initial (maximum) shear strain adjacent to the nose, Z_f is the deformed length of the rod, x' is the normalized position of a point on the rod relative to the nose, and y (x') is the corresponding vertical shear deformation.

Figure 8 includes plastic deformation profiles for L/D = 20 tungsten alloy rods corresponding to a normalized deformed nose mass, j = 1.56, and initial shear strains, γ_θ, of 1 through 4. In plotting the profiles, it is assumed that the one caliber rigid nose piece assumes the slope, γ_θ, of the deformed rod adjacent to the nose and the tail positions for each strain profile are located to preserve the original length of the rod. Within the assumptions of this model, the maximum shear strain occurs adjacent to the nose at the beginning of the deformation. Fracture should

therefore occur at this location when the initial shear strain, γ_θ (Eqn. (19)), exceeds the dynamic fracture shear strain, γ_f (the value for γ_f may actually reflect a tensile failure in some materials). Figure 8 includes a tabulation of measured dynamic fracture shear strains from Ref [7] for a range of more and less ductile materials corresponding to strain rates on the order of 10^2 Sec^{-1}.

Rod deformations and fracture corresponding to the yaw effects plate cutting force are also estimated using the shear deformation model described above. In this case, the cutting force, Fc, tracks down the rod with speed, $\dot{X}$, imparting a transverse velocity, V_T, to the contacted rod segment between X_{ir} and L_r relative to the non-contacted portion. The velocity, V_T, is computed from the impulse-momentum principle assuming impulsive acceleration is resisted by the dynamic shear strength, τ_y. The applied shear stress, τ_c, the initial relative transverse rod velocity, V_T, and the associated shear strain, γ_ϕ, are given by

$$\tau_c = \frac{Fc}{\frac{\pi D^2}{4}}, \qquad V_T = \frac{\tau_c - 2\tau_y}{\rho \dot{x} U_\tau}, \qquad \gamma_\phi = \frac{V_T}{U_\tau} \qquad (21)$$

Failure occurs at the initial contact location if the initial strain exceeds the failure strain, γ_f. If failure does not occur on initial contact, rod deformation is determined by applying the model sketched in Fig. 8 with the effective nose mass, M_n, defined by the smaller of X_i or L_r-X_i and the initial relative velocity, V_T as determined above.

COMPARISONS WITH TEST RESULTS

Model predictions from Eqs 1-15 are compared with measured post-impact trajectory deflections and tumble rates from Ref. [2] in Fig. 9 for titanium rods perforating aluminum plates at normal impact obliquity. The model predicts the increase in trajectory deflections with increasing yaw fairly well and predicts very little difference in trajectory deflections between the L/D = 16 and L/D = 32 rods which is also consistent with the test results. The higher model predictions for the lowest impact speed (1200 m/s) reflect the sensitivity of the transverse loading model to the rod impact speed. That is, the difference between the two sets of curves reflect the counteracting effects of increased impact speed increasing the magnitude of the cutting force while decreasing the duration of the force and the simple geometric decrease in β associated with increasing residual velocity with the same transverse change in velocity. The model properly predicts the steep rise and fall in post-impact tumble rates for both length rods with small increasing impact yaw angles and the lower tumble rates for the longer rod due to its larger transverse moment of inertia. The drop in tumble rates with increasing yaw is due to the decrease in X_{ir} with increasing yaw(Fig. 6). The cutting force effectively tracks along the entire residual rod length for impact yaws greater than about 40° for the shorter rods and 30° for the longer rods.

The FATEPEN code was also exercised to obtain predicted rod responses for comparison with the images in the radiographs in Figs. 1 and 2 (the actual rods were not recovered on these tests). The effective dynamic shear strength and transverse plastic shear wave speed for the tungsten alloy material were determined from Taylor anvil tests and a new transverse wire impact test technique, respectively. The predicted deformed rod profiles were scaled to match the image sizes in the radiographs. The deformed profiles were then overlaid on the radiographs side-by-side with the radiograph images but with the predicted off-shotline excursions and orientations which permits a direct comparison between predicted and observed rod length loss, deformation, trajectory deflection and tumble rate.
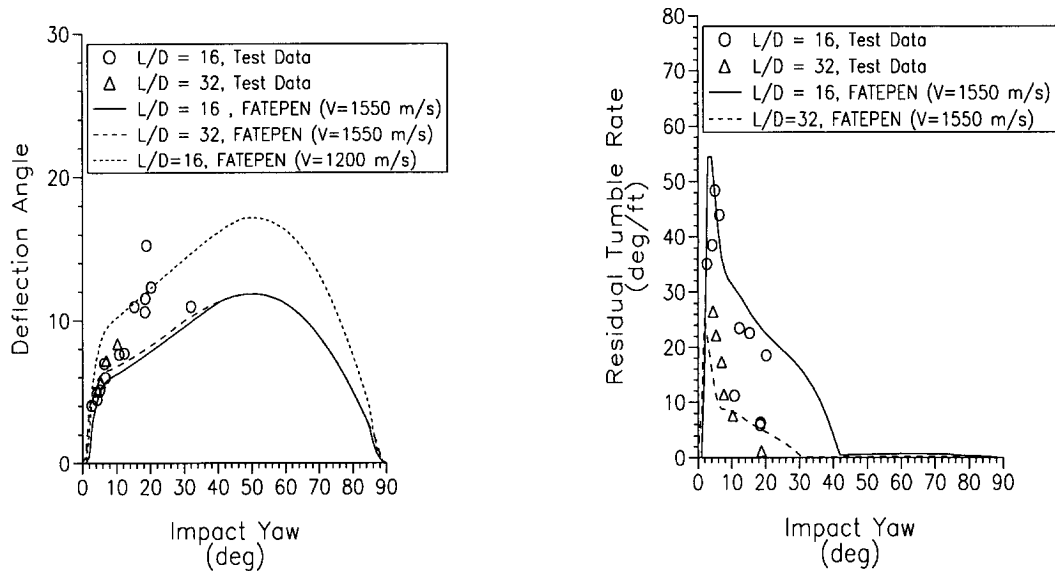
Fig. 9. Post-perforation trajectory deflections and tumble rates for L/D=16 and 32 titanium rods versus 2024-T3 aluminum plates (T/D=1.16), V=1200-1700 m/s, Vavg=1550 m/s, Dt/D=1.84

An overall visual comparison reveals that the model predictions are generally quite realistic The residual rod length and velocity predictions for the normal impacts agreed with the measured values within 2% for residual length and 1% for residual velocity. The effect of increasing yaw on rod deformation, trajectory deflection and tumble rates is also consistent with the radiographs. Note that the predicted images in Fig. 1 correspond to viewing normal to the actual deformation and tumbling plane (i.e., the yaw plane) and thus show slightly more deformation, and rotation then the radiographs which are projections in the vertical or horizontal planes.

The predicted rod images for the 45° impact obliquity correspond to both a predicted obliquity effect (elev. view) and an impact yaw effect delayed contact in the yaw plane. Predicted rod images for the both the obliquity plane and the yaw plane are included and reveal that the tail contact is predicted to cause significant deformation and tumbling in the yaw plane. The predictions could not be confirmed because the post-impact plan view radiographs were not obtained for this test. However, the relatively short predicted elevation view rod image in the second post-impact radiograph indicates the model is over-predicting the yaw plane tumble rate. The model predicts more severe obliquity effect rod deformation and tumbling for the 75° impact obliquity in the lower radiograph of Fig. 2 which is consistent with the radiographs. In this case the tail of the rod is predicted to graze the edge of the hole at a point only 4% from the tail due to the pre-impact yaw. However, this yaw effect is not predicted to cause any deformation and only a 1.5° rotation in the plan view. The actual plan view radiographs confirm no tail deformation but indicate a larger 23° rotation due to the yaw effect. As noted earlier, the apparent counterclockwise rotation in the obliquity plane is attributed to a tail contact due to rod rotation in the plate. The predicted residual length and velocity of the rod in this case agreed with the measurements to within 1% and 3%, respectively.

SUMMARY

New engineering models have been developed to predict rod penetrator transverse loading and response for non-ideal encounter geometries. The models were installed in the FATEPEN penetration code and carefully linked with existing mass and velocity loss models to form a mechanically coupled set of axial and transverse loading and response models for rods penetrating spaced target elements with any combination of impact yaw and obliquity. The combined models predict rod length and velocity losses associated with erosion/extrusion-shear axial loading response mechanisms, and trajectory deflection, post-impact tumbling and rod deformation and fracture due to transverse loading. Comparisons have resulted in good agreement between model predictions and test results for single plate penetration tests involving normal and oblique aluminum and steel plates and titanium and tungsten alloy rods. The improved FATEPEN code should provide more realistic weapons effectiveness assessments resulting in improved rod penetrator warhead designs.

The severity of rod deformation and fracture under a given impulsive transverse loading is determined in large part by the characteristic plastic transverse deformation or shear wave speed, the fracture shear strain, and the dynamic shear strength of the rod material. An improved transverse rod or wire impact test technique was developed as part of the current effort to directly measure these key material parameters from transverse rod deformation profiles versus time recorded by a high speed digital video camera. Planned future work includes additional tests at higher impact speeds to determine critical fracture shear strains and further analyses of the existing deformation profiles to assess the accuracy of the shear wave deformation model presented above

REFERENCES

1. J.D. Yatteau, G.W. Recht, and K.T. Edquist, FATEPEN Rod Penetration Models- Part II, Applied Research Associates, Inc. for Naval Surface Warfare Center, Dahlgren, Virginia (1998)
2. R.H. Zernow, Penetration methodology assessment for titanium rods. Applied Research Associates, Inc. for Naval Surface Warfare Center, Dahlgren, Virginia (1991).
3. J.D. Yatteau, Preliminary tumbling model for long rod penetrators perforating thin plates. Applied Research Associates, Inc. for Naval Surface Warfare Center, Dahlgren, Virginia (1991).
4. J.D. Yatteau, High velocity multiple plate penetration model. Denver Research Institute, University of Denver, for Naval Surface Weapons Center, Dahlgren, Virginia, NSWC-TR-123 (1982).
5. R.F. Recht, High velocity impact dynamics: analytical modeling and plate penetration dynamics. In *High Velocity Impact Dynamics*, (edited by J.A. Zukas),pp. 452-454, John Wiley and Sons, Inc. (1990).
6. R.F. Recht, Taylor ballistic impact modeling applied to deformation and mass loss determinations. *Int. J. Engng. Sci.*, **16**, 809-827 (1978).
7. G.R. Johnson, J.M. Hoegfeldt, U.S. Lindholm, and A. Nagy, Response of various metals to large torsional strains over a large range of strain rates - part 1: ductile metals, part 2: less ductile metals, *ASME J. Engng Mater. Tech.*,**105**(1), 42-53 (1983).